High-Accuracy EMT Simulations through Pole-Residue Compensation

A. A. Kida, A. C. S. Lima, F. A. Moreira, F. M. Vasconcellos

***Abstract*—This paper addresses the frequency warping error in frequency-dependent equivalents to improve the accuracy of Electromagnetic Transient (EMT) simulations. This numerical error, intrinsic to all linear multi-step integration methods, such as the trapezoidal rule, distorts frequency response and degrades time-domain simulation accuracy. This work introduces the Pole-Residue Frequency Warping Compensation (PRFWC) algorithm to mitigate the frequency warping in rational approximations with the pole-residue formulation. Performance validation of the proposed algorithm is conducted through two case studies: a transmission line and a distribution system. Numerical results show that the PRFWC improves simulation accuracy by two orders of magnitude over uncompensated models, with minimal computational burden.**

***Keywords*—Rational Approximation; Pole-residue Formulation; Frequency Warping; Time-Frequency Analysis; Simulation Accuracy.**

I. Introduction

THE increasing complexity of power systems are accelerated by the energy transition from fossil-based to low-carbon and renewable sources [1]. As a result, in-depth analysis of new dynamic interactions between their components and subsystems is paramount [2]. In this context, Electromagnetic Transient (EMT) simulations are an essential tool that can be tuned to provide sufficient accuracy to anticipate these interactions, ensuring reliable and efficient power system planning and operation.

Accurate yet efficient simulations can be achieved by preserving the frequency characteristics of subsystems using frequency-dependent equivalents [3], [4]. A common approach is to represent these equivalents using rational functions derived from data-driven curve-fitting techniques [5], [6], [7]. Vector Fitting (VF) stands out among the curve-fitting techniques for its computational efficiency, accuracy, straightforward formulation, versatility, and open-source availability [5]. Additionally, it is embedded in various EMT-type simulators, including EMTP-ATP [8], EMTDC/PSCAD [9], and EMTP [10].

Time-domain simulations require careful consideration regarding discretization techniques. The trapezoidal rule is widely employed in commercial EMT-type simulators [11] as it is the most accurate among linear multi-step integration methods with A-stability [12].

The continuous-time domain transfer function of the integrator is

$$\frac{b(s)}{u(s)} = \frac{1}{s}, \tag{1}$$

where $b(s)$ and $u(s)$ are the output and the input of the integrator in s-domain, respectively; s is the complex frequency variable in the s-domain.

Applying the trapezoidal rule to derive the transfer function of (1) in the discrete-time domain yields:

$$\frac{B[z]}{U[z]} = \frac{h}{2}\frac{\left(1+z^{-1}\right)}{\left(1-z^{-1}\right)}, \tag{2}$$

where $B[z]$ and $U[z]$ are the Z-transforms of $b(s)$ and $u(s)$, respectively, obtained using the trapezoidal rule; z is the complex variable in the Z-domain.

By equating (1) and (2), then solving for z, yields the bilinear transformation (also known as the Tustin method) [13]:

$$z = \frac{1+0.5sh}{1-0.5sh}. \tag{3}$$

The mapping between the analog (continuous-time) frequency ω_a and its corresponding digital frequency ω is derived by substituting $s = j\omega_a$ and $z = \exp\left(j\omega h\right)$ into (3), where h is the integration time step. Solving for ω_a yields:

$$\omega_a = \frac{2}{h}\tan\left(\frac{\omega h}{2}\right). \tag{4}$$

The nonlinear frequency mapping between ω_a and ω in (4) compresses the discrete-time frequency scale, introducing a numerical error known as frequency warping [14]. This error is not unique to the trapezoidal rule but is inherent to all linear multi-step integration methods [13].

Strategies for frequency warping mitigation mainly involve adjusting the h size, pre-warping, or relying on non-standard solution techniques.

Pre-warping techniques are mostly considered in the context of digital filter design [15], [16], [17]. For instance, a digital frequency specification, such as its cutoff frequency, is prewarped using (4) to build the analog prototype low-pass filter specification, which is then transformed into the desired filter transfer function [15]. Applications of pre-warping for frequency-dependent equivalent (FDE) and power systems are

A. A. Kida is with the Federal Institute of Bahia, Salvador, BA, Brazil (e-mail of the corresponding author: alexandre.kida@ifba.edu.br).

A. C. S. Lima is with the Department of Electrical Engineering of the Federal University of Rio de Janeiro, COPPE/UFRJ, Rio de Janeiro, Brazil (e-mail: acsl@dee.ufrj.br).

F. A. Moreira and F. M. Vasconcellos are with the Department of Electrical and Computer Engineering of the Federal University of Bahia, Salvador, BA, Brazil (e-mails: moreiraf@ufba.br and felipe.vasconcellos@ufba.br).

This research was supported in part by Coordenação de Aperfeiçoamento de Pessoal de Nível Superior (CAPES) under Grant 001, Conselho Nacional de Desenvolvimento Científico e Tecnológico (CNPq) under grants 404068/2020-0, 400851/2021-0, Fundação de Amparo à Pesquisa do Estado de Minas Gerais (FAPEMIG) under grant APQ-03609-17 and Instituto Nacional de Energia Elétrica (INERGE).

Paper submitted to the International Conference on Power Systems Transients (IPST2025) in Guadalajara, Mexico, June 8-12, 2025.

scarce in the literature. In that regard, the author in [18] pre-warped the input frequency response data for a given h before the fitting process. However, this approach cannot be applied to the existing rational approximation, necessitating a model recalculation for different h values.

Concerning h adjustments, adaptive h methods based on energy balance were developed in [19], [20]. However, reducing h might lead to excessive computational overhead. Additionally, [21] proposed the following guideline for h:

$$h \leq \frac{1}{10 f_{max}}, \tag{5}$$

where f_{max} is the highest frequency of interest. However, the authors in [22] showed that frequency warping can still be significant for extended simulation durations, even when h satisfies the criterion in (5).

Non-standard solution techniques, such as the high-order integration method based on the Obreshkov formula, can be applied to mitigate frequency warping [23]. In [14], the authors showed that although the harmonic balance method may encounter convergence issues and performance degradation for signals containing many harmonics, it does not exhibit frequency warping. The main concern with non-standard discretization methods is their lack of extensive documentation, which may lead to unpredictable or undocumented behavior. In contrast, techniques based on the trapezoidal rule are favored for their reliability, stability, and straightforward implementation.

The main contribution of this work is a novel strategy to compensate for the frequency warping caused by the trapezoidal rule, employing rational models based on the pole-residue formulation. Additionally, this work demonstrates how pre-warping inductances and capacitances affect a rational approximation. Finally, the impact of frequency warping on time-domain simulations of frequency-dependent equivalents is highlighted.

This paper is structured as follows. Section II provides the theoretical background for rational approximations, while also complementing the concepts of frequency warping and pre-warping introduced earlier in this paper. Section III details the proposed algorithm. Section IV presents numerical results based on two test cases, providing insights into the performance of the proposed technique. Lastly, key conclusions are drawn in Section V.

II. Discretization Effect of Inductances and Capacitances in a Pole-Residue Formulation

An N-port nodal admittance matrix $\mathbf{Y}(s) \in \mathbb{C}^{N\times N}$ can be approximated by a rational function $\overline{\mathbf{Y}}(s) \in \mathbb{C}^{N\times N}$. Hence,

$$\mathbf{Y}(s) \approx \overline{\mathbf{Y}}(s) = \sum_{i=1}^{N_p} \frac{\mathbf{r_i}}{s - p_i} + \mathbf{D}, \tag{6}$$

where $i \in \{1, \ldots, N_p\}$; $s = j\omega$; ω is the angular frequency in $\mathrm{rad/s}$; N_p is the number of poles or model order; $\mathbf{D} \in \mathbb{R}^{N\times N}$ is the constant term (positive definite matrix); p_i is the i-th pole; $\mathbf{r}_i \in \mathbb{C}^{N\times N}$ is the associated i-th residue matrix.

A single entry m, q of $\overline{\mathbf{Y}}(s)$, $\overline{Y}_{mq}(s)$, can be synthesized using basic circuit components such as resistors, inductors and capacitors [3], as depicted in Fig. 1. Therefore,

$$\begin{aligned}\overline{Y}_{mq}(s) = &\underbrace{\frac{1}{R_0}}_{D} + \underbrace{\sum_{j=1}^{N_{RP}} \frac{1}{R_j + sL_j}}_{\text{Real poles}} \\ &+ \underbrace{\sum_{k=1}^{N_{CP}} \frac{1}{R_k + sL_k + \frac{1}{sC_k + G_k}}}_{\text{Complex poles}},\end{aligned} \tag{7}$$

where D is the constant term; N_{RP}, N_{CP} are the number of real and complex poles of the model, respectively.

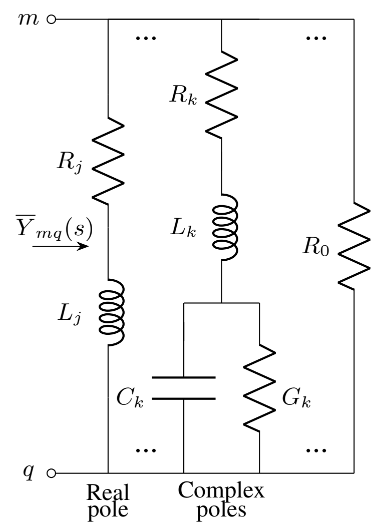

Fig. 1. Electrical network synthesis. Adapted from [3].

A. Frequency-Warping

If the differential network equations are solved using the trapezoidal rule, the capacitances and inductances in (7) become frequency-dependent due to the frequency warping [24]. Therefore,

$$L_{DT}(\omega) = \Psi(\omega) L, \tag{8}$$

$$C_{DT}(\omega) = \Psi(\omega) C, \tag{9}$$

$$\Psi(\omega) = \frac{2}{\omega h} \tan\left(\frac{\omega h}{2}\right), \tag{10}$$

where $L_{DT}(\omega)$ and $C_{DT}(\omega)$ are the discretized inductance L and capacitance C, respectively; the frequency warping error is numerically represented as $\Psi(\omega)$.

B. Pre-Warping

In the discrete-time domain, the expected (analog) behavior of inductors and capacitors for a pre-warping frequency ω' can be retrieved by scaling $L_{DT}(\omega')$ (8) and $C_{DT}(\omega')$ (9) for a factor $\xi(\omega')$. Hence,

$$\xi(\omega') = \frac{1}{\Psi(\omega')} = \frac{\omega' h}{2} \cot\left(\frac{\omega' h}{2}\right), \tag{11}$$

$$L'(\omega') = \xi(\omega')L_{DT}(\omega') = \frac{\omega' h L_{DT}}{2}\cot\left(\frac{\omega' h}{2}\right), \quad (12)$$

$$C'(\omega') = \xi(\omega')C_{DT}(\omega') = \frac{\omega' h C_{DT}}{2}\cot\left(\frac{\omega' h}{2}\right), \quad (13)$$

where $L'(\omega')$ and $C'(\omega')$ are the frequency-warped-compensated inductance and capacitance, respectively.

Consider the complex pole-residue modeled using an RLCG branch [3] depicted in Fig. 1. Therefore, frequency warping can be mitigated by updating $L \leftarrow L'(\omega')$ (12) and $C \leftarrow C'(\omega')$ (13). Thus,

$$\begin{aligned} Y(s) &= \frac{1}{R_1 + sL_1 + \dfrac{1}{sC_1 + G_1}}, \\ &= \frac{sC_1 + G_1}{s^2 L_1 C_1 + s(R_1 C_1 + L_1 G_1) + R_1 G_1 + 1}, \end{aligned} \quad (14)$$

The roots of $Y(s)$ in (14) are its poles p, thus

$$p = \frac{-K \pm \sqrt{K^2 - 4L_1C_1(R_1G_1 + 1)}}{2L_1C_1}, \quad (15)$$

where $K = R_1C_1 + L_1G_1$.

The corresponding residue r of (14)

$$\begin{aligned} r &= \lim_{s\to p}(s-p)Y(s), \\ &= \lim_{s\to p}(s-p)\frac{sC_1 + G_1}{s^2L_1C_1 + sK + R_1G_1 + 1}, \end{aligned} \quad (16)$$

When s approaches p, both numerator and denominator of r in (16) approaches zero. Thus,

$$\begin{aligned} r &= \lim_{s\to p}\frac{\frac{d}{ds}\left[(s-p)(sC_1+G_1)\right]}{\frac{d}{ds}\left(s^2L_1C_1 + sK + R_1G_1 + 1\right)}, \\ &= \lim_{s\to p}\frac{(s-p)C_1 + (sC_1+G_1)}{2sL_1C_1 + K} = \frac{pC_1 + G_1}{2pL_1C_1 + K}. \end{aligned} \quad (17)$$

A frequency-warped-compensated version of (14), denoted as $Y'(s)$, can be obtained by substituting L_1 and C_1 with their corresponding pre-warped versions. Hence,

$$Y'(s) = \frac{1}{R_1 + sL_1'(\omega') + \dfrac{1}{sC_1'(\omega') + G_1}}, \quad (18)$$

By substituting (12) and (13) in (18) and dropping ω' to simplify notation, leads to

$$\begin{aligned} Y'(s) &= \frac{1}{R_1 + s\xi L_1 + \dfrac{1}{s\xi C_1 + G_1}}, \\ &= \frac{s\xi C_1 + G_1}{s^2\xi^2L_1C_1 + s\xi K + R_1G_1 + 1}. \end{aligned} \quad (19)$$

The poles p' of $Y'(s)$ are the roots of its denominator, hence

$$\begin{aligned} p' &= \frac{-\xi K \pm \sqrt{(\xi K)^2 - 4\xi^2L_1C_1(R_1G_1+1)}}{2\xi^2L_1C_1}, \\ &= \frac{-K \pm \sqrt{K^2 - 4L_1C_1(R_1G_1+1)}}{2\xi L_1C_1}. \end{aligned} \quad (20)$$

Thus, by expressing (20) in terms of (15) and recovering the suppressed notation results in

$$p' = \frac{p}{\xi(\omega')}. \quad (21)$$

The corresponding residue r' associated with p' is

$$\begin{aligned} r' &= \lim_{s\to p'}(s-p')Y'(s), \\ &= \lim_{s\to p'}\frac{(s-p')(s\xi C_1 + G_1)}{s^2\xi^2L_1C_1 + s\xi K + R_1G_1 + 1}. \end{aligned} \quad (22)$$

Therefore,

$$\begin{aligned} r' &= \lim_{s\to p'}\frac{\frac{d}{ds}\left[(s-p')(s\xi C_1+G_1)\right]}{\frac{d}{ds}\left(s^2\xi^2L_1C_1 + s\xi K + R_1G_1 + 1\right)}, \\ &= \lim_{s\to p'}\frac{(s-p')C_1 + (s\xi C_1 + G_1)}{2s\xi^2L_1C_1 + \xi K}, \\ &= \frac{p'\xi C_1 + G_1}{2p'\xi^2L_1C_1 + \xi K}. \end{aligned} \quad (23)$$

By substituting (21) in (23) results in

$$r' = \frac{pC_1 + G_1}{2p\xi L_1C_1 + \xi K}. \quad (24)$$

Finally, replacing (17) in (24) and recovering the suppressed notation leads to:

$$r' = \frac{r}{\xi(\omega')}. \quad (25)$$

The scaling of L_1 and C_1 by $\xi(\omega')$, implies scaling of p' and r' by $1/\xi(\omega')$. A similar inference applies to the real pole case (RL branch) using the same methodology outlined in this section.

The pre-warped version of $\overline{\mathbf{Y}}(s)$, denoted as $\overline{\mathbf{Y}'}(s) \in \mathbb{C}^{N\times N}$, is expressed as

$$\overline{\mathbf{Y}'}(s) = \sum_{n=1}^{N_p}\frac{\mathbf{r_i'}}{s - p_i'} + \mathbf{D}, \quad (26)$$

where p_i' and $\mathbf{r_i'}$ represent the i-th pre-warped pole (21) and the matrices of pre-warped residues (25), respectively.

III. The Proposed Algorithm

Choosing an appropriate value for ω' is essential for effective frequency warping mitigation. In the ideal case, the simulated signal contains a single frequency component, allowing ω' to be set to this value, eliminating the frequency warping. However, this scenario is seldom encountered in EMT simulations Furthermore, the precise values of the frequency components in a transient phenomenon are typically unknown before the simulation. Therefore, a more general approach is preferable.

Frequency warping manifests as a disturbance of the original linearized eigenvalues of the simulated system [14]. Although these eigenvalues are typically unknown, frequency response data sampled between ports can be acquired through measurements or simulations. As a result, the equivalent system and its eigenvalues can be approximated (or identified) with a rational approximation through data-driven curve-fitting techniques [5]. The well-known VF [25], [26], [27] approximates the frequency response using a set of poles and residues.

Once the system is identified, the proposed Pole-Residue Frequency Warping Compensation (PRFWC) algorithm pre-warps the pole-residue rational approximation to address the eigenvalue perturbations introduced by frequency warping. The framework for achieving frequency-warped-compensated results with PRFWC as a post-fitting step is shown in Fig. 2. The proposed approach offers an alternative mapping between discrete and continuous-time domains. The algorithm outlined in Pseudocode 1 utilizes the contribution of the imaginary component of each pole in characterizing the oscillatory behavior of a given transfer function. Accordingly, each p_i (21) and $\mathbf{r_i}$ (25) is scaled based on the pre-warping frequency ω_i', such that

$$\omega_i' = \mathbb{I}(p_i), \tag{27}$$

where $\mathbb{I}(p_i)$ is the imaginary frequency component of p_i.

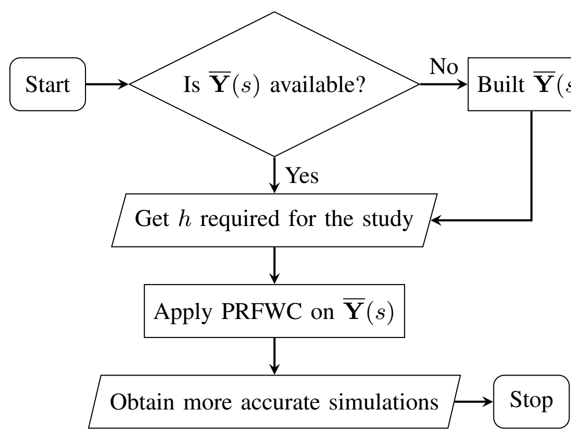

Fig. 2. Proposed framework of PRFWC.

Pseudocode 1 The PRFWC algorithm

for all i **do** ▷ All poles
 $\omega_i' \leftarrow \mathbb{I}(p_i)$ ▷ Eq. (27)
 if $|\omega_i'| < \pi/h$ **then** ▷ Nyquist limit
  $\xi_i \leftarrow (\omega_i' h/2)\cot(\omega_i' h/2)$ ▷ Eq. (11)
  $p_i' \leftarrow p_i/\xi_i$ ▷ Eq. (21)
  $r_i' \leftarrow r_i/\xi_i$ ▷ Eq. (25)
 end if
 $i \leftarrow i + 1$
end for

The proposed algorithm applies strictly to proper rational functions (6), which does not include the s-proportional capacitance term in $\overline{\mathbf{Y}}(\mathbf{s})$. This results from the fact that no single value of ω' can adequately pre-warp this term across the entire frequency range.

IV. Numerical Results and Discussion

The performance of the PRFWC is validated using two frequency-dependent equivalents: a transmission line (Case A) and a distribution network (Case B). The frequency response data used in this work are publicly available on the SINTEF website [28].

The following considerations apply to both cases. The test circuit configuration is illustrated in Fig. 3, with all ports grounded except for port 1. A single voltage source $e(t) = \cos(2\pi f_e t)$ pu applied at port 1 at $t = 0\,\mathrm{s}$. High-frequency transients are simulated with five scenarios, consisting of excitation frequencies f_e varying from $10\,\mathrm{kHz}$ to $90\,\mathrm{kHz}$ in $20\,\mathrm{kHz}$ intervals. The bandwidth of the input frequency response is $10\,\mathrm{Hz}$ to $100\,\mathrm{kHz}$. FDEs are obtained with the VF considering 50 poles. The outputs are the currents $i_j(t)$ for $j = 1, \ldots, N$, following the terminology of the original data in [28], entering the terminals as depicted in Fig. 3. These currents are obtained by convolving the voltage input vector with the FDE and discretizing it using the trapezoidal rule.

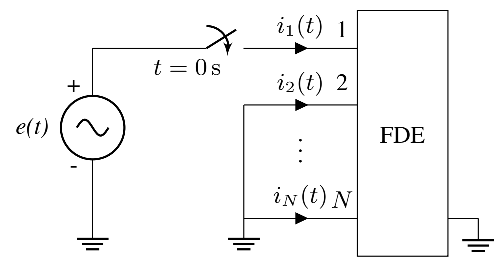

Fig. 3. Test-circuit configuration.

In all scenarios of a given case, $h = 1\,\mu\mathrm{s}$ unless otherwise specified. This value complies with the criterion (5), considering that $f_{max} = 100\,\mathrm{kHz}$ is the highest frequency component of the frequency response data used to build the rational approximation.

In the absence of an analytical solution, a reference waveform $i_{ref}(t)$ is generated by simulating the system with $h = 1\,\mu\mathrm{s}/10000 = 100\,\mathrm{ps}$, as the frequency warping is negligible for such small h.

The accuracy of the proposed algorithm is accessed through two metrics: the relative root mean square error (RRMSE) I_{RRMSE} and the normalized max absolute error (NMAE) I_{NMAE}. The former is a normalized and dimensionless metric of the overall accuracy of the simulation. The latter quantifies the significance of the largest deviation between the simulated and reference signals, normalized by the maximum magnitude of the reference signal. Thus,

$$I_{\mathrm{RRMSE}} = \sqrt{\frac{\sum_{n=1}^{N_T} |i(n) - i_{ref}(n)|^2}{N_T \sum_{n=1}^{N_T} |i_{ref}(n)|^2}}, \tag{28}$$

$$I_{\mathrm{NMAE}} = \frac{\max\left(|i(n) - i_{ref}(n)|\right)}{\max\left(|i_{ref}(n)|\right)}, \tag{29}$$

where $n = t/h$ and N_T is the total number of simulation steps.

The frequency responses presented in this work are directly computed by performing a frequency sweep from $10\,\mathrm{Hz}$ to $100\,\mathrm{kHz}$ on the s-domain rational models $\overline{\mathbf{Y}}(s)$ and $\overline{\mathbf{Y}}'(s)$.

A. Case A: Transmission Line

The first case involves the modeling of a $132\,\mathrm{kV}$ overhead three-phase transmission line, illustrated in Fig. 4. The transmission line is modeled as a three-port frequency-dependent equivalent, with measurements taken at the sending-end of the line while the receiving-end of the line is open-circuited. The dc resistance per unit length is $0.121\,\Omega/\mathrm{km}$ for the phase wire and $0.359\,\Omega/\mathrm{km}$ for the ground wire. The line length is $12\,\mathrm{km}$. The diameters of the phase and ground wires are $21.66\,\mathrm{mm}$ and $12.33\,\mathrm{mm}$, respectively. The soil resistance is $100\,\Omega\,\mathrm{m}$. The output is the current at port 1 $i_1(t)$, considering the configuration shown in Fig. 3.

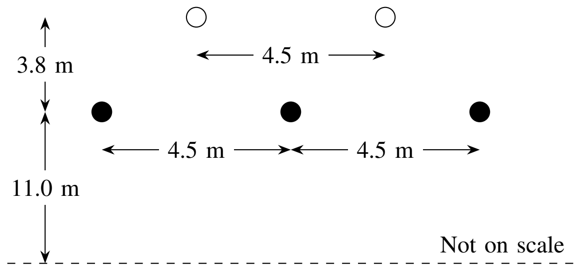

Fig. 4. 132 kV three-phase transmission line conductor configuration, Case A. The ground and phase wires are represented as white and black circles, respectively. Adapted from [29].

PRFWC altered the original frequency response in the frequency domain to compensate for the distortion imposed by frequency warping as depicted in Fig. 5. The most noticeable differences between the frequency responses manifest at higher frequencies, where the frequency warping exerts a more substantial compressing effect. Likewise, poles with larger imaginary parts underwent significant pre-warping, as illustrated in Fig. 6.

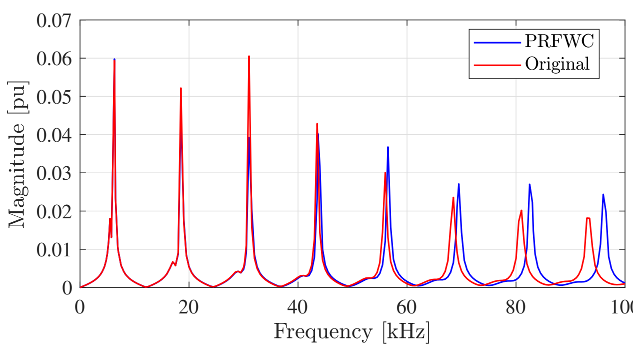

Fig. 5. Magnitude of frequency responses, Case A.

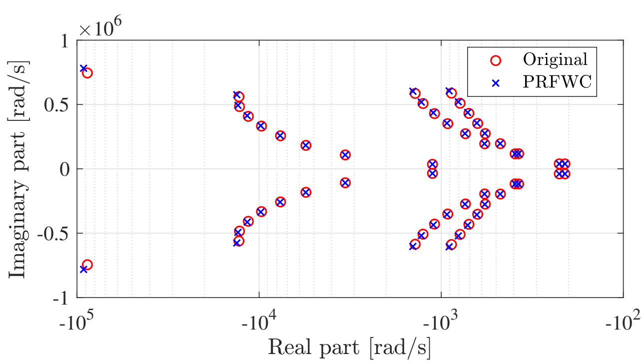

Fig. 6. Pole placement of the rational approximations, Case A.

Table I provides quantitative evidence of the substantial error reduction through the simulation achieved in all tested scenarios by the proposed method. The accuracy improvement is of two orders of magnitude across all evaluated scenarios. The RRMSE of the PRFWC with $h = 1\,\mu\mathrm{s}$ is comparable to the original (uncompensated) signal with $h = 1\,\mu\mathrm{s}/4 = 250\,\mathrm{ns}$, as presented in Table II. Table III demonstrates that the PRFWC method reduced the worst-case deviation by one to two orders of magnitude across all scenarios, as quantified by the NMAE metric. Notably, the uncompensated waveforms exhibited NMAE values as high as 249.26%, whereas the PRFWC methodology achieved a significantly lower value of 10.71%.

TABLE I
RRMSE VALUES FOR TIME-DOMAIN SIMULATIONS ACROSS ALL SCENARIOS IN CASE A

f_e (kHz)	PRFWC (%)	Original (%)	Ratio†
10	2.89×10^{-2}	7.37×10^{-1}	3.92×10^{-2}
30	3.87×10^{-2}	5.67×10^{-1}	6.82×10^{-2}
50	1.71×10^{-1}	3.05	5.61×10^{-2}
70	9.96×10^{-2}	3.48	2.86×10^{-2}
90	3.60×10^{-1}	1.20×10^{1}	2.99×10^{-2}

†RRMSE of PRFWC over original.

TABLE II
RRMSE VALUES FOR TIME-DOMAIN SIMULATIONS ACROSS ALL SCENARIOS IN CASE A, USING A REDUCED TIME-STEP FOR THE ORIGINAL SIMULATION

f_e (kHz)	PRFWC (%)	Original* (%)	Ratio†
10	2.89×10^{-2}	3.89×10^{-2}	7.43×10^{-1}
30	3.87×10^{-2}	2.01×10^{-2}	1.93
50	1.71×10^{-1}	1.22×10^{-1}	1.40
70	9.96×10^{-2}	1.77×10^{-1}	5.63×10^{-1}
90	3.60×10^{-1}	3.48×10^{-1}	1.03

*With h reduced from $1\,\mu\mathrm{s}$ to $250\,\mathrm{ns}$.
†RRMSE of PRFWC over original with $h = 250\,\mathrm{ns}$.

TABLE III
NMAE FOR TIME-DOMAIN SIMULATIONS ACROSS ALL SCENARIOS IN CASE A

f_e (kHz)	PRFWC (%)	Original (%)	Ratio†
10	2.61	25.17	1.04×10^{-1}
30	1.35	23.53	5.74×10^{-2}
50	5.26	73.91	7.12×10^{-2}
70	4.32	89.71	4.82×10^{-2}
90	10.71	249.26	4.30×10^{-2}

†NMAE of PRFWC over original.

On the qualitative side, the time-domain waveforms for f_e values of $50\,\mathrm{kHz}$ and $90\,\mathrm{kHz}$ are displayed in Figs. 7 and 8, respectively. It is clear that, even for the same h, the original waveform exhibited significant deviations from the reference, whereas the PRFWC results closely matched the reference.

For the $50\,\mathrm{kHz}$ source, the frequency warping increased the amplitude of the original waveform in Fig. 7 around $0.15\,\mathrm{ms}$, $0.30\,\mathrm{ms}$ and $0.45\,\mathrm{ms}$. In contrast, the amplitude of the original signal was reduced around 0.35 ms. This behavior can be understood by analyzing the spectrum near 50 kHz in Fig. 5. Depending on the frequency, the amplitude of the original frequency response may be either lower or higher than that obtained with PRFWC. Lastly, Fig. 8 demonstrates that for $f_e = 90\,\text{kHz}$, frequency warping led to significant amplitude errors of the original signal after 0.1 s. This effect can be interpreted as the result of the mapping imposed by frequency warping, which shifts the original resonance peak with the highest frequency in Fig. 5 to a value closer to f_e.

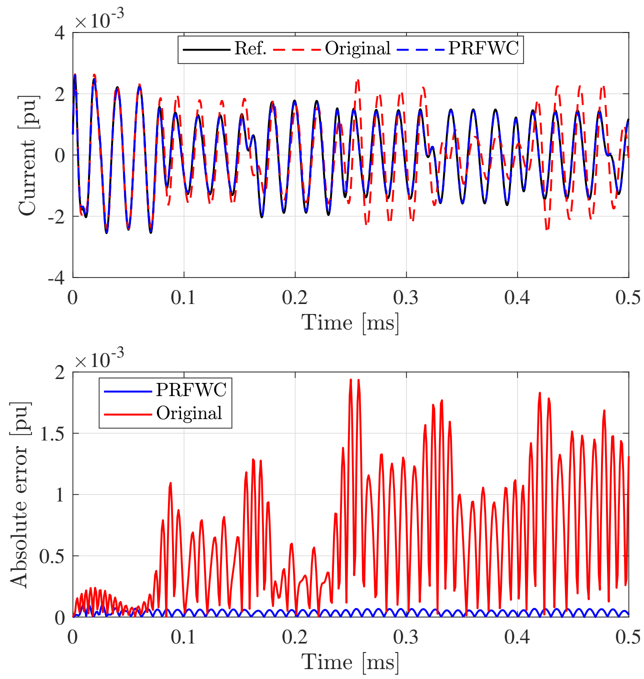

Fig. 7. Time-domain responses of the reference, original and PRFWC waveforms (top), along with their absolute error (bottom) with $f_e = 50\,\text{kHz}$, Case A.

B. Case B: Distribution Network

The second case, illustrated in Fig. 9 represents a two three-phase buses (A and B) distribution network modeled as a six-port FDE. $\overline{\mathbf{Y}}(s)$ is computed regarding both bus-bars. The output is evaluated as the current at port 2 $i_2(t)$, following the configuration shown in Fig. 3.

As illustrated in Fig. 10, the PRFWC approach modified the original frequency response to alleviate the compression effects induced by frequency warping. As expected, the spectral components at higher frequencies underwent more significant pre-warping. This trend is further validated by analyzing the pole placement generated by the proposed algorithm in Fig. 11.

The PRFWC attained an accuracy improvement of two orders of magnitude across all scenarios, as outlined in Table IV. Moreover, the uncompensated signal only reached a comparable level of accuracy to the PRFWC when h was decreased from 1 µs to 250 ns as shown in Table V. For Case B, Table VI highlights that the PRFWC method decreased the NMAE by one to two orders of magnitude across all scenarios. Remarkably, uncompensated waveforms showed NMAE values reaching 128.54%, whereas the proposed approach achieved a significantly lower value of 14.10%.

Time-domain waveforms for $f_e = 10\,\text{kHz}$ and $f_e = 90\,\text{kHz}$ are shown in Figs. 12 and 13, respectively. Although

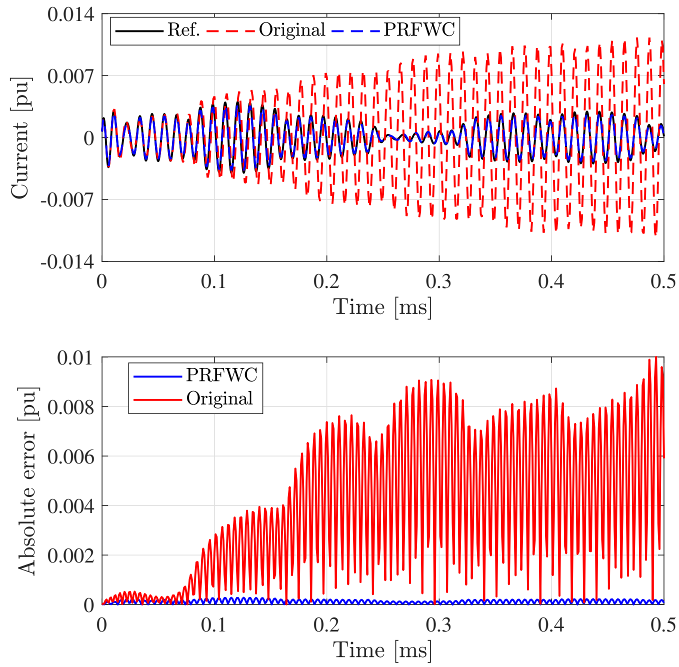

Fig. 8. Time-domain responses of the reference, original and PRFWC waveforms (top), along with their absolute error (bottom) with $f_e = 90\,\text{kHz}$, Case A.

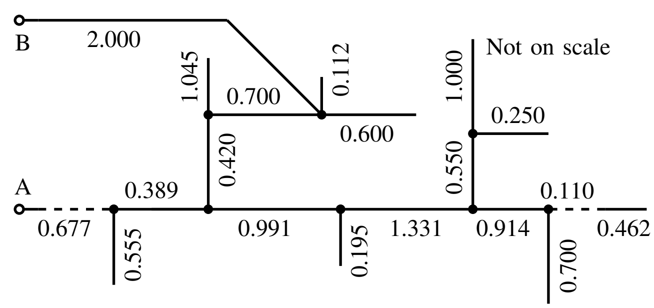

Fig. 9. Single-line diagram of the three-phase distribution system, Case B. The numbers are the line length in km. Continuous and dashed lines are overhead lines and underground cables, respectively. Adapted from [30].

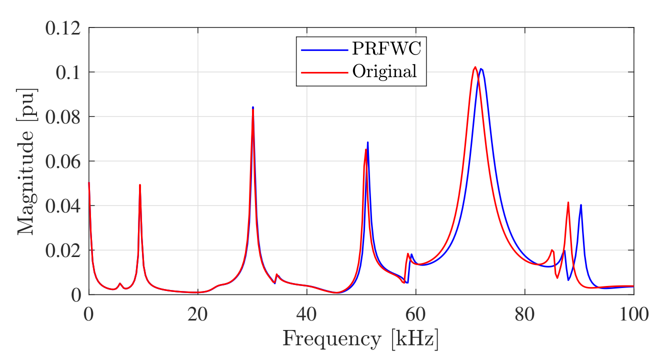

Fig. 10. Magnitude of frequency responses, Case B.

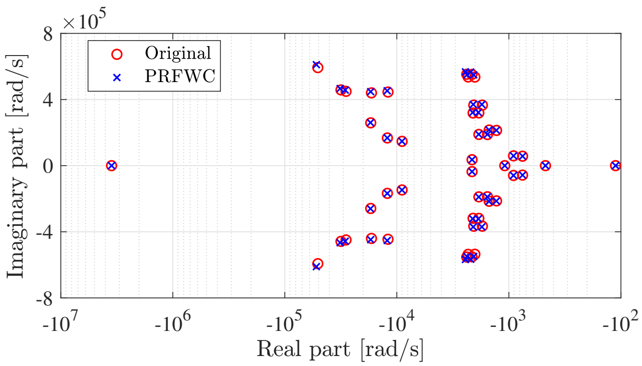

Fig. 11. Pole placement of the rational approximation, Case B.

TABLE IV
RRMSE VALUES FOR TIME-DOMAIN SIMULATIONS ACROSS ALL SCENARIOS IN CASE B

f_e (kHz)	PRFWC (%)	Original (%)	Ratio†
10	5.03×10^{-2}	6.04×10^{-1}	8.33×10^{-2}
30	3.50×10^{-2}	4.83×10^{-1}	7.26×10^{-2}
50	8.56×10^{-2}	2.18	3.93×10^{-2}
70	2.30×10^{-1}	5.24	4.40×10^{-2}
90	2.74×10^{-1}	4.53	6.04×10^{-2}

†RRMSE of PRFWC over original.

TABLE V
RRMSE VALUES FOR TIME-DOMAIN SIMULATIONS ACROSS ALL SCENARIOS IN CASE B, USING A REDUCED TIME-STEP FOR THE ORIGINAL SIMULATION

f_e (kHz)	PRFWC (%)	Original* (%)	Ratio†
10	5.03×10^{-2}	6.20×10^{-2}	8.12×10^{-1}
30	3.50×10^{-2}	2.01×10^{-2}	1.74
50	8.56×10^{-2}	1.22×10^{-1}	7.02×10^{-1}
70	2.30×10^{-1}	1.77×10^{-1}	1.30
90	2.74×10^{-1}	3.48×10^{-1}	7.87×10^{-1}

*With h reduced from $1\,\mu$s to 250 ns.
†RRMSE of PRFWC over original with $h = 250$ ns.

TABLE VI
NMAE VALUES FOR TIME-DOMAIN SIMULATIONS ACROSS ALL SCENARIOS IN CASE B

f_e (kHz)	PRFWC (%)	Original (%)	Ratio†
10	9.14	14.68	6.23×10^{-1}
30	3.07	11.80	2.60×10^{-1}
50	4.69	62.41	7.51×10^{-2}
70	5.50	128.54	4.28×10^{-2}
90	14.10	124.96	1.13×10^{-1}

†NMAE of PRFWC over original.

the PRFWC and the original magnitude frequency response in Fig. 10 match well around 10 kHz, the time-domain response in Fig. 12 shows a noticeable deviation from the reference between 0.1 ms and 0.3 ms. In contrast, Fig. 13 shows a significant distortion of the original waveform, particularly between 0.2 ms and 0.3 ms, while the PRFWC signal closely matches the reference. This discrepancy is caused by the frequency warping shifting the original resonance peak with the highest frequency in Fig. 10 to a value lower than the excitation frequency.

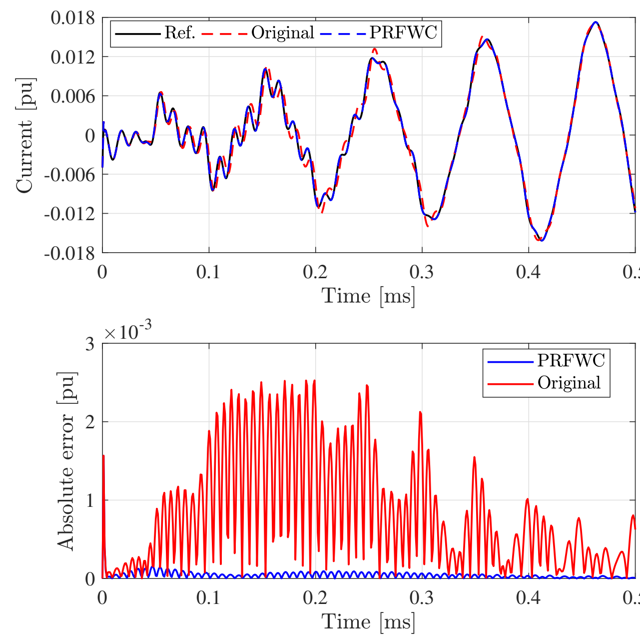

Fig. 12. Time-domain responses of the reference, original, and PRFWC waveforms (top), along with their absolute error (bottom) with $f_e = 10$ kHz, Case B.

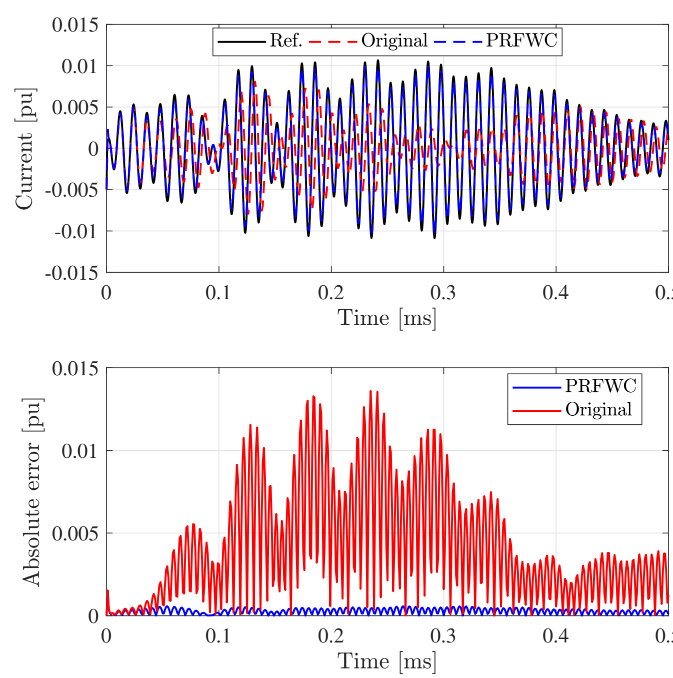

Fig. 13. Time-domain responses of the reference, original, and PRFWC waveforms (top), along with their absolute error (bottom) with $f_e = 90$ kHz, Case B.

C. Discussion

The numerical results show that frequency warping can significantly affect EMT solutions, even when h satisfies (5), particularly for the frequency responses with resonance peaks. The oscillation of the absolute error arises from the amplitude error, which is more pronounced at peak values and less severe near zero values.

PRFWC consistently reduced the frequency warping, enhancing accuracy by two orders of magnitude in all scenarios. The uncompensated waveform required a much smaller h, with a 1:4 ratio compared to the h used for the PRFWC, to achieve comparable results to those obtained with the proposed method. Consequently, the uncompensated simulation needed at least four times as many numerical model evaluations as those obtained with PRFWC. Notably, this improvement incurs negligible computational overhead, as the scaling factors are computed only once per pole and residue.

V. Conclusions

This paper examined the numerical error known as frequency warping in electromagnetic transient simulations of frequency-dependent equivalents. The Pole-Residue Frequency Warping Compensation (PRFWC) method effectively improves the accuracy of rational approximations based on the pole-residue formulation. With its negligible computational overhead, the PRFWC provides a more efficient alternative to reducing the time-step size to improve simulation accuracy. Its simple implementation, high computational efficiency, and enhanced accuracy make it well-suited for integration in data-driven curve-fitting techniques as a post-processing routine.

References

[1] F. M. Gonzalez-Longatt, "Activation schemes of synthetic inertia controller on full converter wind turbine (type 4)," pp. 1–5, 2015.

[2] Y. Ji and Y. Xing, "Highly accurate and efficient time integration methods with unconditional stability and flexible numerical dissipation," *Mathematics*, vol. 11, no. 3, 2023.

[3] B. Gustavsen, "Rational approximation of frequency-dependent admittance matrices," *IEEE Transactions on Power Delivery*, vol. 17, no. 4, pp. 1093–1098, 2002.

[4] T. Noda, "Identification of a multiphase network equivalent for electromagnetic transient calculations using partitioned frequency response," *IEEE Transactions on Power Delivery*, vol. 20, no. 2, pp. 1134 – 1142, Apr. 2005.

[5] S. Grivet-Talocia and B. Gustavsen, *Passive Macromodeling: Theory and Applications*, ser. Wiley Series in Microwave and Optical Engineering. New York, US: John Wiley & Sons, 2015, vol. 239.

[6] T. Campello, F. Dicler, S. Varricchio, H. de Barros, C. Costa, A. Lima, and G. Taranto, "Reviewing the large electrical network equivalent methods under development for electromagnetic transient studies in the brazilian interconnected power system," *International Journal of Electrical Power & Energy Systems*, vol. 151, p. 109033, 2023.

[7] B. Salarieh and H. De Silva, "Review and comparison of frequency-domain curve-fitting techniques: Vector fitting, frequency-partitioning fitting, matrix pencil method and Loewner matrix," *Electric Power Systems Research*, vol. 196, p. 107254, 2021.

[8] H. K. Høidalen, "Atpdraw news," 2024. [Online]. Available: https://www.atpdraw.net/news.php

[9] B. Gustavsen and J. Nordstrom, "Pole identification for the universal line model based on trace fitting," *IEEE Transactions on Power Delivery*, vol. 23, no. 1, pp. 472 –479, Jan. 2008.

[10] J. Naredo, J. Mahseredjian, J. Gutierrez-Robles, O. Ramos-Leaños, C. Dufour, and J. Belánger, "Improving the numerical performance of transmission line models in emtp," in *Proceedings of the International Conference on Power Systems Transients*, Jun. 2011, pp. 1–8.

[11] A. Ametani, *Numerical Analysis of Power System Transients and Dynamics*, ser. Energy Engineering. UK: Institution of Engineering and Technology, 2015.

[12] G. G. Dahlquist, "A special stability problem for linear multistep methods," *BIT*, vol. 3, no. 1, pp. 27–43, 1963.

[13] W. Y. Yang, T. G. C. I. H. Song, Y. S. C. J. Heo, W. G. Jeon, and J. W. L. J. K. Kim, *Signals and Systems with MATLAB*. Berlin, Heidelberg: Springer, 2009.

[14] A. Brambilla and G. Storti-Gajani, "Frequency warping in time-domain circuit simulation," *IEEE Transactions on Circuits and Systems I: Fundamental Theory and Applications*, vol. 50, no. 7, pp. 904–913, 2003.

[15] L. Tan, *Digital Signal Processing: Fundamentals and Applications*, 1st ed. Decatur, Georgia: Academic Press, 2008.

[16] L. L. Presti, "Prewarping techniques in filter simulation by bilinear transformation," *Signal Processing*, vol. 5, no. 6, pp. 523–529, 1983.

[17] W. Teng, X. Zhang, Y. Zhang, and L. Yang, "Iterative tuning notch filter for suppressing resonance in ultra-precision motion control," *Advances in Mechanical Engineering*, vol. 8, no. 11, p. 1687814016674097, 2016.

[18] F. Dicler, "Contributions to the FPGA and CPU implementation of Frequency-Dependent Network Equivalents for real-time and offline electromagnetic transient power system simulators," Master's thesis, PEE/COPPE/UFRJ, Nov. 2021.

[19] A. G. Gheorghe, F. Constantinescu, and M. Nitescu, "Error control in circuit transient analysis," in *2009 16th IEEE International Conference on Electronics, Circuits and Systems - (ICECS 2009)*, Dec. 2009, pp. 207–210.

[20] F. Constantinescu, A. G. Gheorghe, and M. Niţescu, "The energy balance error for circuit transient analysis," *Revue Roumaine des Sciences Techniques, Série Électrotechnique et Énergétique*, vol. 54, no. 3, pp. 243–250, 2010.

[21] J. Marti and J. Lin, "Suppression of numerical oscillations in the EMTP," *IEEE Transactions on Power Systems*, vol. 4, no. 2, pp. 739–747, 1989.

[22] A. Kida, A. Lima, F. Moreira, J. Martí, and J. Tarazona, "Inaccuracies due to the frequency warping in simulation of electrical systems using combined state–space nodal analysis," *Electric Power Systems Research*, vol. 223, p. 109657, 2023.

[23] K. Gao, "A study in the frequency warping of time-domain methods," Master, University of Ottawa, Ottawa, 2015.

[24] H. W. Dommel, *Electromagnetic Transients Program Reference Manual (EMTP Theory Book)*, B. P. Administration, Ed. Branch of System Engineering - Bonneville Power Administration, 1995.

[25] B. Gustavsen and A. Semlyen, "Rational approximation of frequency domain responses by vector fitting," *IEEE Transactions on Power Delivery*, vol. 14, no. 3, pp. 1052–1061, 1999.

[26] B. Gustavsen, "Improving the pole relocation properties of vector fitting," *IEEE Transactions Power Delivery*, vol. 21, no. 3, pp. 1587–1592, Jul. 2006.

[27] D. Deschrijver, M. Mrozowski, T. Dhaene, and D. De Zutter, "Macromodeling of multiport systems using a fast implementation of the vector fitting method," *IEEE Microwave and Wireless Components Letters*, vol. 18, no. 6, pp. 383–385, 2008.

[28] B. Gustavsen, "The Vector Fitting website," 2008. [Online]. Available: https://www.sintef.no/projectweb/vectorfitting/

[29] ——, "Fast passivity enforcement for pole-residue models by perturbation of residue matrix eigenvalues," *IEEE Transactions on Power Delivery*, vol. 23, no. 4, pp. 2278–2285, 2008.

[30] D. Deschrijver, B. Gustavsen, and T. Dhaene, "Advancements in iterative methods for rational approximation in the frequency domain," *IEEE Transactions on Power Delivery*, vol. 22, no. 3, pp. 1633–1642, 2007.